HHS Public Access

Author manuscript

Mol Cell. Author manuscript; available in PMC 2014 April 15.

Published in final edited form as:

Mol Cell. 2010 March 12; 37(5): 702–713. doi:10.1016/j.molcel.2010.02.003.

Collaborative Dynamic DNA Scanning by Nucleotide Excision Repair Proteins Investigated by Single-Molecule Imaging of Quantum-Dot-Labeled Proteins

Neil M. Kad[1,*], **Hong Wang**[2,3], **Guy G. Kennedy**[4], **David M. Warshaw**[4], and **Bennett Van Houten**[2,3,*]

[1]Department of Biological Sciences, University of Essex, Colchester, Essex CO4 3SQ, UK

[2]Department of Pharmacology and Chemical Biology, University of Pittsburgh School of Medicine, University of Pittsburgh, Pittsburgh, PA 15213, USA

[3]The University of Pittsburgh Cancer Institute, Hillman Cancer Center, University of Pittsburgh, Pittsburgh, PA 15213, USA

[4]Department of Molecular Physiology & Biophysics, University of Vermont, Burlington, VT 05405, USA

SUMMARY

How DNA repair proteins sort through a genome for damage is one of the fundamental unanswered questions in this field. To address this problem, we uniquely labeled bacterial UvrA and UvrB with differently colored quantum dots and visualized how they interacted with DNA individually or together using oblique-angle fluorescence microscopy. UvrA was observed to utilize a three-dimensional search mechanism, binding transiently to the DNA for short periods (7 s). UvrA also was observed jumping from one DNA molecule to another over ~1 μm distances. Two UvrBs can bind to a UvrA dimer and collapse the search dimensionality of UvrA from three to one dimension by inducing a substantial number of UvrAB complexes to slide along the DNA. Three types of sliding motion were characterized: random diffusion, paused motion, and directed motion. This UvrB-induced change in mode of searching permits more rapid and efficient scanning of the genome for damage.

INTRODUCTION

One of the fundamental questions in the field of DNA repair is how a modest number of repair proteins scan through several million (for bacteria) to a few billion (for mammalian cells) base pairs of nondamaged DNA to find rare damaged bases. How proteins locate their cognate recognition sequences has been extensively studied over the years (von Hippel and Berg, 1986, 1989), and several modes of searching have been hypothesized and recently

*Correspondence: nkad@essex.ac.uk (N.M.K.), vanhoutenb@upmc.edu (B.V.H.).

SUPPLEMENTAL INFORMATION

Supplemental Information includes Supplemental Experimental Procedures, Supplemental Data, Supplemental Calculations, Supplemental References, six figures, and ten movies and can be found with this article online at doi:10.1016/j.molcel.2010.02.003.

reviewed (Gorman and Greene, 2008). It is generally believed that facilitated diffusion in a one-dimensional (1D) search greatly enhances the rate of site location. However, direct sliding along DNA could be hampered by the numerous proteins bound to DNA inside a living cell. Thus, other searching modes such as hopping or intersegmental transfer have been proposed.

Nucleotide excision repair (NER) is a generalized DNA repair system capable of recognizing and removing a diverse array of chemical and physical DNA lesions, such as UV-induced photoproducts and carcinogen-DNA adducts (Batty and Wood, 2000; Friedberg et al., 1995, 2006; Sancar, 1996). This highly conserved process is mediated by the concerted action of several proteins. NER is initiated by DNA distortion detection and then followed by: (1) damage verification, (2) coordinated incisions, (3) excision of an oligonucleotide containing the damaged base, (4) repair synthesis, and (5) ligation. In humans, a deficiency in any one of the 7 out of the ~30 NER proteins required for efficient repair can lead to the syndrome xeroderma pigmentosum, characterized by high incidence of skin cancer and, in some cases, neurodegeneration (Lehmann, 2001; Takayama et al., 1996).

UvrA and UvrB are the proteins that mediate damage recognition during NER (Goosen and Moolenaar, 2001; Sancar and Rupp, 1983; Truglio et al., 2006a; Van Houten et al., 2005). Approximately 20–50 copies of UvrA and UvrB are normally found per *E. coli* cell; however, SOS response induction mediated by LexA results in a further 5- to 10-fold induction of the UvrA and UvrB proteins (Sancar and Sancar, 1988). The crystal structures and function analysis of UvrA (Pakotiprapha et al., 2008), UvrB (Machius et al., 1999; Nakagawa et al., 1999; Sohi et al., 2000; Theis et al., 1999; Truglio et al., 2006b; Waters et al., 2006), and UvrC (Karakas et al., 2007; Truglio et al., 2005) have helped delineate the molecular interactions and action mechanism of each protein during the coordinated damage recognition and repair process.

UvrA as a dimer interacts with UvrB to form either a $UvrA_2B$ or $UvrA_2B_2$ complex (Orren and Sancar, 1990; Verhoeven et al., 2002; Wang et al., 2006); for simplicity, we refer to these complexes as UvrAB hereafter. During damage recognition UvrA is hypothesized to recognize helical distortions induced in the DNA rather than the actual modified nucleotide (DellaVecchia et al., 2004; Van Houten et al., 2005). UvrA initiates damage verification through derepression of an autoinhibitory domain (domain 4) (Wang et al., 2006) on UvrB (Truglio et al., 2006b). UvrB engages the damaged site through a β-hairpin, causing dissociation of UvrA (Truglio et al., 2006b). UvrC then binds, producing dual incisions surrounding the damage (Truglio et al., 2006a; Van Houten et al., 2005). In the final steps of NER, DNA polymerase I and UvrD (helicase II) remove the postincision complex and synthesize the repair patch, which is sealed by DNA ligase (Caron et al., 1985; Husain et al., 1985). Despite the structural and biochemical information available about these proteins, the dynamics of these interactions on DNA remain elusive. To help elucidate this problem, we have turned to single-molecule approaches (Wang et al., 2006, 2008), which have previously been successfully employed for the study of other DNA protein systems, including EcoRV diffusion on DNA (Bonnet et al., 2008); Rad51 involved in recombination (Granéli et al., 2006); hOgg1, a glycosylase involved in base excision repair (Blainey et al., 2006); and the action of mismatch repair heterodimer of Msh2-Msh6 (Gorman et al., 2007).

In this present study, we have created a robust visualization platform for protein-DNA interactions at the single-molecule level. Specifically, using highly fluorescent quantum dots (Qdots) to label individual UvrA and UvrB molecules, we observed the interactions and molecular movements of these proteins on λ-DNA "tightropes." Based on this approach, we report here that damage recognition during NER involves an initial 3D search by UvrA, which collapses into a 1D search when UvrB is added. Unexpectedly, we have found that UvrAB has a complex motion on DNA and appears to display unbiased diffusion, directed motion, and paused motion. Finally, differential labeling of both UvrA and UvrB with different color Qdots has uniquely allowed direct visualization of a protein complex of two separate protein partners loading onto DNA and dissociating during the process of NER.

RESULTS

To achieve single-molecule resolution of repair protein interactions with DNA, we developed a holistic approach to overcome the three key imaging limitations: (1) fluorescence signal intensity and prevention of fluorophore photobleaching, (2) isolation of the DNA from the surface, and (3) reduction of background signals. This was achieved in three stages. First, we labeled our proteins with Qdot nanocrystals (Figure 1A), which possess high quantum yields, can be excited by a continuum of wavelengths, and are highly resistant to photobleaching. Second, we raised the DNA above the surface using a "DNA tightrope" assay (Figure 2A). This permitted the DNA to be visualized extended rather than in its usual collapsed form (Movie S1). Furthermore, potential interactions with the surface that would alter protein migration on the DNA could be eliminated. Such artifacts may be present with techniques that directly apply the DNA to a surface. Third, the architecture of the DNA platform necessitated the application of a unique illumination strategy to reduce background fluorescence.

Qdot Conjugation and UvrA/UvrB Activity

To observe proteins interacting with the DNA tightropes, we conjugated Qdots to UvrA and UvrB proteins (see Supplemental Information). We have previously reported on a Qdot conjugation strategy for UvrB. A nine-residue HA tag was added to UvrB's N terminus, which was subsequently conjugated to the Qdot via an antibody sandwich (Wang et al., 2008) (Figure 1A). In order to avoid cross-reactivity, we used a second strategy to conjugate Qdots to UvrA. BirA biotin ligase was used to attach biotin, with greater than 90% efficiency (data not shown), to a C-terminally engineered biotin ligase recognition sequence on UvrA (Chapman-Smith and Cronan, 1999). AFM was used to directly observe the UvrA-Qdot conjugates and to quantify the stoichiometry of biotinylated UvrA (UvrA-bio) binding to the streptavidin-coated Qdots at the single-molecule level. Qdots exhibit a homogeneous, symmetrical shape (Figure 1B). Since there are several streptavidin molecules attached to each Qdot (Qdot Streptavidin Conjugates User's Manual, Invitrogen), it was essential to find conditions that ensured the binding of only one UvrA dimer per Qdot. This was achieved by using a 5-fold excess of Qdots over UvrA-bio. After incubation of UvrA-bio with streptavidin-coated Qdots (Figure 1C), AFM images showed particles in close proximity to the Qdots (Figure 1C, orange arrow). Furthermore, statistical analyses of AFM images

indicated that approximately 15% of the Qdots (n = 85) carried these particles, and no more than one particle was in close proximity to a Qdot.

To investigate whether or not UvrA-Qdot conjugates can still bind to DNA, agarose-based EMSAs were used in which Qdots and protein-Qdot conjugates can enter the gel matrix (Wang et al., 2008). EMSAs were performed with a 50 bp duplex DNA substrate containing a fluorescein-adducted thymine (Croteau et al., 2006) at the central position on the top strand (see Supplemental Information). A representative agarose gel assessing DNA binding of UvrA-bio before and after Qdot conjugation is shown in Figure 1D (right panel). Streptavidin-coated Qdots (in the absence of UvrA) did not interact with DNA (Figure 1D, left panel). UvrA- and UvrA-Qdot DNA complexes were clearly resolved under our agarose-EMSA conditions. At 20 and 50 nM protein concentrations, ~19% and 29% of the DNA was bound by UvrA-bio, respectively, which is comparable with results obtained using WT UvrA. After conjugation to Qdots, UvrA-Qdot bound to DNA to a similar extent as compared with unconjugated UvrA-bio (right panel of Figure 1D, compare lane 4 with 2 and lane 5 with 3). It is worth noting that under the same conditions, we observed 1:1 formation of UvrA-Qdot (Figure 1C). These results indicate that 1:1 conjugation of UvrA to Qdots does not significantly interfere with DNA binding by UvrA. In addition, EMSA assays also confirmed that conjugation of UvrA to a Qdot does not affect UvrB loading onto damaged DNA (Figure 1E, compare lane 7 with 6).

DNA Tightropes and the Interaction between Qdot-Labeled UvrA and DNA

To visualize the Qdot-labeled proteins, we constructed DNA tightropes (Figures 2A and 2B) by sequentially flowing through the construction materials as outlined in the Experimental Procedures (see Movie S2). Extended DNA was bound to 5 μm beads, elevating them from the surface, which not only prevented interactions of the Uvr proteins with the surface but also assisted in identifying when Uvr-Qdot proteins were bound. Any fluorescence in the focal region must derive from proteins bound to DNA and not the surface, which was out of the focal plane. Figure 2C shows the same region of tightropes as Figure 2B after the addition of 655 nm (red) Qdot-labeled UvrA. A number of red fluorescent spots appear on the DNA, each corresponding to a single UvrA molecule conjugated to a Qdot (Movie S3). As a control, Qdots were not observed to attach to the DNA in the absence of conjugation to UvrA (data not shown).

The experimental approach developed here results in the binding of numerous Uvr protein-conjugated Qdots throughout the visual field (x, y coordinate) at any point in time. To characterize all potential binding events throughout the entire visual field, we developed a simple “streak analysis” that assessed both the duration and mode of binding. This method of data presentation involves taking an intensity profile along a specified line through every frame in the movie, hence creating a movie of kymographs (described in Supplemental Information and Movie S4).

Briefly, this very simple transposition of the data set dimensions (x, y space through time is converted to x, t space through y increments) permits an extremely simple, rapid, and accurate analysis of the data from many molecules. Measuring the lengths of the lines, “time streaks” associated with the appearance and disappearance of a Qdot in each frame provide

the lifetime of the interaction between the Qdot-labeled molecule and DNA. In addition, since the DNA is reasonably well aligned to the horizontal axis of the frame, any Qdot motions along the DNA will result in nonhorizontal streaks, yielding information about movement. Directed motion appears as a sloped time streak, whereas unbiased random walks appear as undulating time streaks (see Figure 3A for example time streaks).

Figure 3B shows the duration of interaction for 337 UvrA molecules in three separate experiments obtained from streak analysis of horizontal time streaks (Figure 3A, top panel), which is indicative of a bound, nonmotile UvrA. The lifetimes were binned and plotted as a histogram to reveal an exponential character expected for a single stochastic process that limits release of the molecule from the DNA. A second exponential is also seen; however, due to its very small amplitude, it was not examined further in this study. From this analysis, the rate of detachment from the DNA is 0.14 (± 0.01) s^{-1}, equivalent to a residence time of ~7 s.

Surprisingly, very few of the UvrA encounters with DNA (less than 5%) exhibited any motion, i.e., nonhorizontal time streaks. Qdots were considered motile if their corresponding time streaks showed at least one clear change in position; based on these criteria, ~5% of streaks showed movement. However, less than 1% of molecules showed any clear continuous motion on the DNA. Despite this lack of sliding, we observed UvrA molecules jumping from one DNA duplex to another without an apparent return to bulk solution (Movie S5). Qdot positions were tracked using the MTrackJ (ImageJ plugin). It is interesting to note that this intermolecular “jumping” did not require the two DNA helices to be in direct contact, with a resulting mean translocation distance of 1.2 (± 0.1 SEM [steps]) μm (n = 51 molecules and 190 steps). Long-range translocations were scored when a Qdot disappeared and then reappeared in the next frame (t = 483 ms). The low concentration of UvrA-Qdots in these experiments makes the binding of a different UvrA molecule from the solution pool unlikely (see calculation in Supplemental Information). Indeed, no differences in the total incidence of UvrA jumping from one DNA strand to another were apparent with flowcells that had all free UvrA flushed from the flowcell.

Stoichiometry of UvrAB Interactions

Given the unique dual-color labeling strategy employed here, we were able to address a key question in the field: the stoichiometry of the UvrAB interaction. First, we evaluated the oligomeric states of UvrAB by capturing complexes formed in the absence of DNA on a surface and then imaging using total internal reflectance fluorescence microscopy (TIRFM). We observed very few colocalized red ($Qdot_{655nm}$) and green ($Qdot_{565nm}$) Qdots (2.7%) in the absence of protein (Table 1). We labeled UvrB with red and green Qdots such that only one Qdot was bound per protein molecule; in the absence of UvrA, we saw little colocalization (7.7%). However, in the presence of UvrA, UvrB formed dual-colored complexes (21%), indicating that UvrA facilitates the formation of a complex containing two molecules of UvrB. We also studied the formation of complexes on DNA tightropes; both UvrA individually and UvrB (in the presence of UvrA) formed dual-colored complexes on DNA (33% and 25%, respectively). These data indicate that under the conditions of our experiments, UvrB is mostly a monomer, and two independent molecules can bind to a

UvrA dimer to form a $UvrA_2B_2$ complex. This is in agreement with bulk methods using FRET (Malta et al., 2007) and is consistent with the recent structures of the UvrA-UvrB interface domains (Pakotiprapha et al., 2008, 2009).

The Effect of UvrB on the Binding of UvrA to DNA

Based on the dwell time data of UvrA alone and the known inefficiency of 3D searching (Halford and Szczelkun, 2002; Slutsky and Mirny, 2004; von Hippel and Berg, 1989), it would appear that UvrA is incapable of sampling ample genomic DNA prior to bacterial cell division (for calculations, see Supplemental Information). We therefore sought to assess the effects of its known binding partner UvrB. UvrB could increase UvrA's rate of DNA sampling by two methods: (1) reduce the dwell time spent at any one site, or (2) collapse the 3D search into a 1D search.

We have previously shown that Qdot-conjugated UvrB interacts with and can be loaded onto DNA by UvrA (Wang et al., 2008). To ascertain that the same interaction exists in our present experimental system, we performed a simple control experiment: Qdot-conjugated UvrB was incubated with or without Qdot-conjugated UvrA before being loaded into the flowcell. UvrB-conjugated Qdots were observed to bind to the DNA only when UvrA was present (data not shown). Additionally, in a dual-color experiment, red Qdot-conjugated UvrB was observed to load onto DNA preloaded with green UvrA-Qdot, suggesting the preformation of UvrAB complexes in solution was not essential. Lastly, even in the absence of DNA, UvrA was seen to coordinate the association of two UvrB molecules to form the UvrAB complex (Table 1). These observations confirm that Qdot-conjugated UvrB interacts with Qdot-conjugated UvrA.

To determine how UvrB alters the binding of UvrA to DNA, we applied two complementary approaches using untagged and Qdot-conjugated wild-type UvrB. Both approaches gave identical rates, and these data were therefore combined. Figure 4A shows a histogram of UvrA interactions in the presence of UvrB. No apparent change in the rate of detachment was observed (0.14 s^{-1} versus 0.13 s^{-1}). To further assess how UvrB affects UvrA's interaction with DNA, we performed a titration of UvrB against a constant concentration of UvrA. Figure 4B shows a compilation of rates derived from exponential fits to lifetime histograms similar to that shown in Figure 4A at differing UvrB concentrations. Interestingly, the apparent rate of UvrA's detachment from DNA was not increased by the presence of UvrB. While these data suggest that UvrB does not influence the off rate of nonmoving UvrA molecules from DNA, we did detect a remarkable change in the number of motile protein molecules (see below). When the lifetimes of only these motile complexes were examined in isolation, an increase in the residence time on DNA to ~40 s was revealed (Figure 4C).

The Motion of UvrAB Complexes on DNA

In the presence of UvrB, UvrA exhibited a statistically significant (chi-square test; $p < 0.001$) 3-fold higher probability of movement (~17% versus ~5%), suggesting that the UvrAB complex is more motile. Of 1221 observed interactions between UvrAB complexes and DNA, 213 (17%) moved greater than 125 nm (one pixel), and 1008 remained static,

representing a large increase in the number of motile complexes versus UvrA alone. Of these motile complexes, 36 of their time streaks were of sufficient duration (at least five frames) to be analyzed in detail. We noted three types of motion (Figure 3A): (1) 61% of the motile molecules showed free diffusion (n = 22), where the protein-Qdot complex varied randomly in position (Figure 3Ab and Movie S6); (2) 19% of the motile molecules showed directed motion (n = 7), where the protein-Qdot complexes were observed to possess directionality and hence were sloped (Figure 3Ac [top molecule] and Movie S7); and (3) 19% of the motile molecules displayed paused motion (n = 7), which was characterized by long pauses followed by short bursts of movement (Figure 3Ad and Movie S8). The mean squared displacement (MSD) of each freely diffusing UvrAB complex (category one) was plotted against time in Figure 5A. The average slope provided the diffusion constant calculated as 4.4 (± 0.2) × 10^{-4} $\mu m^2 s^{-1}$.

The second and third categories of motile molecules demonstrated a bias to their motion, consistent with directed motion or motion under flow. There was no imposed flow during observations, and the direction of the movement did not necessarily correlate with the former flow direction. Therefore, it is likely that the mode of binding is altered to facilitate directed motility. A representative MSD plot of this motion is shown in Figure 5B; the upward curvatures for all such plots were best fitted to a second-order polynomial. The coefficients of the quadratic and linear terms represent the velocity of directed motion and twice the 1D diffusion constant, respectively. From such fits, the mean rate of UvrAB complex-directed movement was 1.3 (± 0.5 SEM) × 10^{-3} μms^{-1} (~4 bps^{-1}) in addition to a mean unbiased diffusive component of 2.3 (± 1.2 SEM) × 10^{-3} $\mu m^2 s^{-1}$.

Paused motion (Figure 3Ad [bottom] and Movie S8) was not clearly correlated to the protein-labeling strategy used. When plotted as an MSD versus time, this motion showed curvature similar to that seen in Figure 5B; however, clearly not all upwardly curved plots showed paused motion. Furthermore, paused motion was not seen in those data possessing linear MSD plots (Figure 5A), consistent with free diffusion. To understand paused motion further, we simulated 100 unbiased diffusers with randomly located pauses exponentially distributed around a number of lifetimes. The average MSD plot from these simulations was linear, albeit with a reduced diffusion constant, giving no indication of the pauses contained in the data (see Supplemental Information). Therefore, MSD plot curvature associated with molecules undergoing paused motion is not due to pauses, indicating that the pauses occur preferentially in the directed-motion data set.

UvrAB Complex Motility in the Absence of ATP

The current models for bacterial NER suggest an important role for ATP in UvrA dimer formation that increases UvrA's affinity for DNA (Goosen and Moolenaar, 2001). Furthermore, it is believed that ATP is absolutely required for productive UvrAB interaction and subsequent binding to a damaged site (Goosen and Moolenaar, 2001; Orren and Sancar, 1989; Truglio et al., 2006a). In this study so far, 1 mM ATP was used in all of the previous experiments with UvrB; therefore, we assessed the role of ATP by examining the binding of UvrA to DNA and the formation of UvrAB complexes in the absence of ATP. Consistent with previous work (Mazur and Grossman, 1991), in the absence of ATP, considerable static

binding to DNA of UvrA was observed (data not shown). Furthermore, ATP was not required for the formation of dual-labeled UvrAB complexes or their subsequent association with the DNA. Thus, in contrast to bulk assays where the end points are productive, binding to a site-specific lesion in a DNA substrate, we found that ATP was unnecessary to form a UvrAB complex that is capable of binding to DNA. Also, in the absence of ATP, UvrAB was capable of motion unlike UvrA alone without ATP. It was found that 29% (± 1 SEM, n = 50 movers) of all imaged interactions showed some movement. Of all dual-labeled complexes containing one labeled UvrA and one labeled UvrB, 39% (± 0.3 SEM, n = 22 movers) showed movement in the absence of ATP. These data indicate that at the single-molecule level, ATP is apparently not required to form the UvrAB complex or for diffusively scanning DNA. It is possible, however, that some residual ATP may remain in the active sites of UvrA or UvrB. None of the moving molecules showed any directed motion, consistent with ATP acting as the energy source for this mode of motion, shown in Figure 5B.

DISCUSSION

The search for a lesion in DNA presents a considerable challenge to a repair system, since the damage site is tethered in a linear array and surrounded in three dimensions by nontarget DNA at very high local concentrations. This study sheds light on how the NER proteins UvrA and UvrB address this problem. By using a unique DNA tightrope assay that permits direct visualization of the interaction of a large ensemble of these Qdot-conjugated proteins with DNA, we have shown that UvrA forms a dimer that is capable of bringing together two UvrB molecules both on and off DNA. On DNA, the association with UvrB switches the UvrAB search mechanism so that a much larger proportion of molecules participate in a 1D diffusional search. These observations have uncovered another damage recognition role for UvrB, which is to activate sliding on DNA. By individually labeling UvrA with one color Qdot and UvrB with a second color, we have directly visualized complex formation and composition in real time (Movie S9).

UvrB Affects How UvrA Interacts with DNA

Without UvrB present, UvrA employs a 3D random search mechanism, where it binds DNA for ~7 s before releasing and rebinding elsewhere. UvrA was also found to jump a mean distance of 1.2 μm between DNA molecules without returning to bulk solution, offering an alternative mechanism for accelerating the rate of diffusional encounter. This compares well to a previous study imaging the motion of EcoRV (Bonnet et al., 2008), but is in contrast with the few other enzymes examined using single-molecule techniques and that are known to utilize a 1D search mechanism (Blainey et al., 2006; Gorman et al., 2007; Kabata et al., 1993; Tafvizi et al., 2008).

The interaction of UvrAB with DNA becomes more complicated since both nonmotile and motile complexes were observed. The residence time of the former on DNA remained at ~7 s regardless of the ratio of UvrB to UvrA. This important observation suggests that UvrB does not alter the mechanism of UvrA's detachment from DNA. Conversely, the observed motile UvrAB complexes exhibited a 6-fold increase in their residence time on DNA.

Therefore, UvrB changes UvrA's mode of interaction from a nonmotile to a sliding molecule and at the same time alters how the UvrAB complex dissociates from DNA. It is important to note that for successful analysis of sliding velocities, we could only examine the longer records, biasing our assessment to longer lifetimes; therefore, the 6-fold increase in attached lifetime is an upper estimate. Nonetheless, a change in mode and mechanism of UvrA's interaction with DNA is evident. However, why only a fraction (17%) of the molecules enter a search mode is unclear at present. It is possible that the binding equilibrium between UvrA and UvrAB is not saturated; however, no clear correlation was observed between the ratio of UvrB to UvrA and the number of motile molecules in Figure 4B (data not shown).

For those molecules that enter a search mode, we calculated the diffusion constant from a linear fit to the MSD versus time plot yielding 4.4×10^{-4} $\mu m^2 s^{-1}$. The maximum theoretical diffusion constant for Qdot-labeled UvrAB complex (Stokes radius of ~13.5 nm) spiraling along the groove of DNA and therefore experiencing rotational as well as translational friction is calculated as 2.1×10^{-2} $\mu m^2 s^{-1}$ (Schurr, 1979). This value is ~50-fold greater than our observed value, indicating that the UvrAB complex encounters large energy barriers to free motion. We have calculated the energy barrier assuming the UvrAB complex steps by 1 bp along the DNA as 3.9 $\kappa_B T$ (see Supplemental Information). This energy barrier is considerably higher than the predicted 2 $\kappa_B T$ for efficient target location (Slutsky and Mirny, 2004). Although it is still possible that the complex is performing small "hops" to the next binding site (von Hippel and Berg, 1986, 1989), we assume these large barriers to motion exist as a consequence of the complex attempting to slide along the DNA. The high energy barrier to free sliding may be the result of the UvrAB complex causing significant structural alterations in the DNA as it scans for damage. Since the free energy barrier is 1.9 $\kappa_B T$ higher than efficient searching would predict (Slutsky and Mirny, 2004), it is necessary to recalculate how long it would take these complexes to scan a bacterial genome. Based on our observed diffusion constant of 4.4×10^{-4} $\mu m^2 s^{-1}$ for the Qdot-conjugated UvrAB complex, we calculate the distance scanned per encounter with the DNA for the UvrAB complex (after removing the Qdot contribution; see Supplemental Information) as ~2.5 kbp. Therefore, in order for the genome to be scanned, a single UvrAB complex in an *E. coli* cell would need to make ~1200 encounters with the DNA; if each encounter lasts 40 s, then the genome would be scanned in ~13 hr! Therefore, to scan the genome within the doubling time for *E. coli* at 37°C of 20 min, ~40 complexes would be required. This value is comparable to estimates for the number of complexes present in the cell. During the SOS response, more Uvr proteins are present and cell division is delayed, offering a greater opportunity to locate damage.

Comparison of UvrAB with Other DNA Repair Systems

It is of interest to compare the behavior of the damage recognition proteins involved in NER studied here using single-molecule motility assays with other repair proteins, including base excision repair glycosylases and mismatch repair proteins. T4 pyrimidine dimer glycosylase (PDG, formerly endonuclease V) has been shown to be highly processive at nicking DNA containing pyrimidine dimers, both in vitro and in vivo (reviewed in (Lloyd, 2005). These results would imply that T4 PDG, after acting on one pyrimidine dimer, is capable of sliding

some distance to another dimer site. In addition, in vivo experiments with the UvrABC system suggested similar processivity (Lloyd, 2005). Recently, hOgg1 and Msh2-Msh6 have been examined using single-molecule approaches (Blainey et al., 2006; Gorman et al., 2007). Both systems exhibited much faster 1D diffusion constants (5.8×10^{-1} $\mu m^2 s^{-1}$ and 1.2×10^{-2} $\mu m^2 s^{-1}$, respectively), but also shorter interaction times than those reported here (0.025 and 10.2 s, respectively). Interestingly, despite these differences in diffusion constants and dwell times, the overall length of DNA scanned per encounter is similar between UvrAB, hOgg1, and Msh2-Msh6.

The UvrAB Complex Is Not Always Engaged in a Random Walk

In addition to the 1D diffusional motion, one-third of all the observed motile molecules in our study showed slow but directed motion. Quantitative examination of the motion of these molecules showed that the MSD plots did not accurately fit to a quadratic relationship, expected for directed motion, but instead fit well to a combination of 1D diffusion and directed motion. The combination of these two modes in one search strategy may be taken to mean that UvrAB diffuses between slow ~4 bp/s steps or, alternatively, may suggest a "burning bridges" Brownian ratchet model (Saffarian et al., 2004). While this motion could not increase the overall rate of the search, it could help facilitate identification of a damaged site in the vicinity of the DNA encounter. UvrAB complexes were also observed to pause during their motion in a process termed here "paused motion." None of these pauses occurred during unbiased diffusion, but instead were limited to those molecules exhibiting directed motion. Furthermore, Monte Carlo simulations suggested that the paused motion did not generate the characteristic curvature of a directed mover. Therefore, paused motion may also represent a functional process associated with UvrAB complexes checking DNA for deformities associated with damage. Quantitative PCR data (Figure S1) suggest that the λ-DNA used in these experiments possess on average three sites of damage. These damaged sites may explain some of the heterogeneity of the motile complexes. Additionally, the macromolecular composition of the UvrAB complex may also contribute to the observed heterogeneity of protein motion. We have determined here that the UvrAB complex is largely $UvrA_2B_2$; however, some amount of $UvrA_2B$ is also likely to be present. We are currently engaged in linking the heterogeneity of these behaviors to both the complex composition and the presence of damage by incorporating damage into known regions of the DNA.

The Role of ATP

Through a large number of biochemical studies, it has been shown that both UvrA and UvrB consume ATP. While several hypotheses have been posited to explain the ATPase activity of UvrA and UvrB (Goosen and Moolenaar, 2001; Skorvaga et al., 2004; Truglio et al., 2006a), a definitive mechanism of action has not been realized. We find that by omitting ATP, UvrA was able to bind DNA in much the same manner as in the presence of ATP. This indicates that ATP is not necessary for binding of UvrA to DNA as previously suggested (Wagner et al., 2009). Furthermore, unlike previous bulk biochemical studies, UvrA was also capable of loading UvrB onto DNA in the absence of ATP. Therefore, our present studies indicate that ATP does not play a significant role in the association of UvrA or UvrAB with DNA. However, there was a substantial increase in the number of motile

UvrAB complexes (from 17% to 29%) in the absence of ATP. As expected, in the absence of an external energy source, this motion did not appear directed. These data indicate that the presence of ATP alters the energy barriers to motion. One potential explanation of this is that ATP induces the helicase fold of UvrB to clamp down on the DNA, stalling further motion. Studies to investigate this are currently underway.

Structural Speculations on the Binding of UvrA and UvrAB to DNA

The NER mechanism is extremely versatile in its function, being able to remove a large variety of DNA adducts. The rich conformational complexity of the UvrAB proteins provides diverse interactions with DNA. We have found that UvrA binds to DNA as a dimer and displays no movement at the resolution of our experiments; however, UvrAB complexes are clearly more mobile on DNA. As discussed above, the energy barrier for a UvrAB complex making 1 bp steps along the DNA is 3.9 $\kappa_B T$. This energy barrier could be due to structural alterations in both the proteins and DNA. Indeed, the zinc fingers of UvrA are believed to make direct contact with the DNA (Croteau et al., 2006), and binding of UvrA to DNA causes a site-specific bend of 40–60°, as observed by atomic force microscopy (H.W. and B.V.H., unpublished data). This transient DNA bend at the site of the lesion may help facilitate opening of the DNA, allowing damage verification by UvrB (DellaVecchia et al., 2004). UvrB's helicase fold is coupled to a β-hairpin that makes direct contact with the DNA (Truglio et al., 2006b), which could be processing the DNA in an energy-requiring step during damage searching. Thus, we believe that the UvrAB complex dynamically samples the DNA's conformational state as it slides along the DNA. These motile UvrAB complexes would be expected to make fewer DNA contacts; therefore, it is surprising to note that they remain attached to the DNA for a longer period of time (40 s on average). Therefore, the decrease in the energy barrier to diffusing along the DNA is not reflected in a decrease of the energy barrier to detachment; rather, it would appear to show the opposite. To achieve this, UvrAB may form a ring around the DNA, such that with UvrB, UvrA binds more weakly but is topologically restrained from leaving the DNA. In high ionic strength conditions, UvrAB-Qdot complexes and also UvrA-Qdot alone were observed to slide rapidly along the DNA (0.25 [± 0.12] $\mu m^2 s^{-1}$; discussed in more detail in the Supplemental Information). The measured diffusion constants were greater than theoretically possible for rotational diffusion along the DNA groove. Therefore, the protein-Qdot complexes at high salt slide linearly along the DNA, ignoring the groove contour; this is consistent with the formation of a ring-like complex.

In summary, this study has demonstrated that UvrA can interact with DNA, forming nonmotile complexes with or without ATP (Figure 6 and Movie S10). This interaction does not efficiently search the genome and therefore may serve to keep UvrA within the vicinity of DNA. However, in the presence of UvrB, the central molecule of NER, the UvrAB complex becomes capable of performing a 1D search for damage as well as a 3D random binding search, greatly increasing the efficiency of locating lesions. With greater amounts of UvrB present during the SOS response, this mechanism links the activation of NER to the detection of DNA damage. We have found that the UvrAB complex employs multiple mechanisms in its 1D search, suggesting that there is considerable conformational flexibility in the Uvr damage search and recognition apparatus, perhaps underlying its ability to

recognize structurally unrelated DNA adducts. Extending these studies to real-time imaging in the presence of DNA lesions and UvrC will permit a much clearer view of this complex mechanism. Indeed, given the similarities between UvrB and the eukaryotic NER protein XPD (Wolski et al., 2008), it is conceivable that the mechanisms revealed using this method of visualizing DNA-protein interactions will be shared across all families of life.

EXPERIMENTAL PROCEDURES

Experimental Conditions

All imaging experiments were performed in imaging buffer consisting of 50 mM Tris-HCl (pH 7.5), 50 mM KCl, 10 mM $MgCl_2$, 100 mM DTT, and 1 mM ATP (except in the minus-ATP experiments). The high DTT concentration prevented excessive photobleaching of the dye. This was preferred to oxygen scavenger systems used previously (Kad et al., 2003), since we have observed solution aggregates and incomplete elongation of the DNA under flow in their presence. DTT (100 mM) was confirmed by EMSA assays to have no effect on the formation of the preincision complex (data not shown). Qdots were used as described in the text and were always kept in excess to ensure only a single Uvr protein was attached to each Qdot (Wang et al., 2008). Experiments were performed at room temperature, and images were taken at various frame rates. Qdots were conjugated to UvrA through a streptavidin-biotin linkage and to UvrB through a HA-primary-secondary-Qdot sandwich (Supplemental Information).

DNA Tightrope Assay

Target site location for DNA repair proteins requires sorting through large stretches of nontarget DNA. In solution, DNA forms dynamic bundles (Movie S1), limiting visualization of protein-DNA interactions. Therefore, to investigate these properties, the DNA needs to be physically elongated, and this was achieved by suspending λ-DNA between 5 μm beads to form “DNA tightropes.”

These tightropes were constructed using a flowthrough chamber (flowcell; see Supplemental Information) that allowed each solution to be passed over a polyethylene-$glycol_{5000}$ (PEG)-blocked surface. Despite this blocking, 5 μm poly-L-lysine-coated beads could randomly adhere to the PEG surface when passed into the flowcell. λ-DNA was subsequently flowed into the chamber for suspension between beads (Figure 2 and Movie S2). YOYO-1 dye was added after formation of DNA tightropes to facilitate locating the DNA strands in the field of view. Furthermore, this concentration of YOYO-1 dye was not found to affect the binding of UvrA and UvrB in ensemble assays. Figure 2B shows a typical visual field of DNA tightropes. Many adjacent tightropes are visible, creating a linear network of DNA akin to the high local concentrations of DNA present in vivo. Furthermore, this network permitted the observation of multiple DNA-protein interactions simultaneously. Another benefit of this assay is that there is no interaction between the DNA and the surface, which could interfere with the activity of the proteins. In addition, since flow was not imposed after setting up the tightropes, this enables detection of multiple modes of interaction, such as jumping from one DNA molecule to another and DNA sliding (Gorman and Greene, 2008). In many

experiments, after confirming that the DNA molecules were attached to the beads, the YOYO-1 dye was washed free using 1XABC buffer.

Streak Analysis

To enable analysis of both dwell times of Qdot-labeled proteins and their modes of interaction with the DNA, we developed a process termed “streak analysis.” This process consisted of three steps: (1) masking of bead pedestals, (2) event detection, and (3) data analysis (these are summarized in Movie S4).

Masking—To eliminate the contribution of Qdots bound to the poly-L-lysine-coated bead pedestals, we manually masked the 5 μm spheres from the field of view.

Event Detection—This approach consisted of creating kymograph time streak movies of the Uvr protein-Qdot conjugate interacting with λ-DNA strung between beads.

Data Analysis—These time streak movies were inspected frame by frame (i.e., in the y-dimension) to ascertain the period and the mode of binding. To address the effects of Qdot blinking, a streak was regarded as the same molecule if it disappeared and reappeared in the same location, since the probability of a binding event at the same location was considered negligible.

Supplementary Material

Refer to Web version on PubMed Central for supplementary material.

Acknowledgments

We thank Samantha Beck for technical assistance, Andrew Dunn for discussions and measurements of flow rates, and M.D. Yusuf Ali and the rest of the Warshaw lab for critical discussions. We also thank Susan Wallace and Alan Chant at the University of Vermont for their crucial support in the early stages of this project. We thank Dorothy Erie at the University of North Carolina at Chapel Hill for her suggestions and AFM instrument time, and we also thank Harshad Ghodke for help in preparing some of the proteins used in this study. Finally, we wish to thank the reviewers for their very helpful suggestions that improved the quality of this study. This work was supported by NIEHS/NIH intramural program, UPCI-startup (B.V.H.), DB007A7 (N.M.K.), The Royal Society (DB3HR6 to N.M.K.), and National Institutes of Health Grants HL059408, HL085489 (D.M.W.), and K99ES016758-01 (H.W.).

References

Batty DP, Wood RD. Damage recognition in nucleotide excision repair of DNA. Gene. 2000; 241:193–204. [PubMed: 10675030]

Blainey PC, van Oijen AM, Banerjee A, Verdine GL, Xie XS. A base-excision DNA-repair protein finds intrahelical lesion bases by fast sliding in contact with DNA. Proc Natl Acad Sci USA. 2006; 103:5752–5757. [PubMed: 16585517]

Bonnet I, Biebricher A, Porté PL, Loverdo C, Bénichou O, Voituriez R, Escudé C, Wende W, Pingoud A, Desbiolles P. Sliding and jumping of single EcoRV restriction enzymes on non-cognate DNA. Nucleic Acids Res. 2008; 36:4118–4127. [PubMed: 18544605]

Caron PR, Kushner SR, Grossman L. Involvement of helicase II (uvrD gene product) and DNA polymerase I in excision mediated by the uvrABC protein complex. Proc Natl Acad Sci USA. 1985; 82:4925–4929. [PubMed: 3161077]

Chapman-Smith A, Cronan JE Jr. The enzymatic biotinylation of proteins: a post-translational modification of exceptional specificity. Trends Biochem Sci. 1999; 24:359–363. [PubMed: 10470036]

Croteau DL, DellaVecchia MJ, Wang H, Bienstock RJ, Melton MA, Van Houten B. The C-terminal zinc finger of UvrA does not bind DNA directly but regulates damage-specific DNA binding. J Biol Chem. 2006; 281:26370–26381. [PubMed: 16829526]

DellaVecchia MJ, Croteau DL, Skorvaga M, Dezhurov SV, Lavrik OI, Van Houten B. Analyzing the handoff of DNA from UvrA to UvrB utilizing DNA-protein photoaffinity labeling. J Biol Chem. 2004; 279:45245–45256. [PubMed: 15308661]

Friedberg, EC.; Walker, GC.; Siede, W. DNA repair and mutagenesis. Washington, DC: ASM Press; 1995.

Friedberg, EC.; Walker, GC.; Seide, W.; Wood, RD.; Schultz, RA.; Ellenberger, T. DNA Repair and Mutagenesis. Washington, DC: ASM Press; 2006.

Goosen N, Moolenaar GF. Role of ATP hydrolysis by UvrA and UvrB during nucleotide excision repair. Res Microbiol. 2001; 152:401–409. [PubMed: 11421287]

Gorman J, Greene EC. Visualizing one-dimensional diffusion of proteins along DNA. Nat Struct Mol Biol. 2008; 15:768–774. [PubMed: 18679428]

Gorman J, Chowdhury A, Surtees JA, Shimada J, Reichman DR, Alani E, Greene EC. Dynamic basis for one-dimensional DNA scanning by the mismatch repair complex Msh2-Msh6. Mol Cell. 2007; 28:359–370. [PubMed: 17996701]

Granéli A, Yeykal CC, Robertson RB, Greene EC. Long-distance lateral diffusion of human Rad51 on double-stranded DNA. Proc Natl Acad Sci USA. 2006; 103:1221–1226. [PubMed: 16432240]

Halford SE, Szczelkun MD. How to get from A to B: strategies for analysing protein motion on DNA. Eur Biophys J. 2002; 31:257–267. [PubMed: 12122472]

Husain I, Van Houten B, Thomas DC, Abdel-Monem M, Sancar A. Effect of DNA polymerase I and DNA helicase II on the turnover rate of UvrABC excision nuclease. Proc Natl Acad Sci USA. 1985; 82:6774–6778. [PubMed: 2931721]

Kabata H, Kurosawa O, Arai I, Washizu M, Margarson SA, Glass RE, Shimamoto N. Visualization of single molecules of RNA polymerase sliding along DNA. Science. 1993; 262:1561–1563. [PubMed: 8248804]

Kad NM, Rovner AS, Fagnant PM, Joel PB, Kennedy GG, Patlak JB, Warshaw DM, Trybus KM. A mutant heterodimeric myosin with one inactive head generates maximal displacement. J Cell Biol. 2003; 162:481–488. [PubMed: 12900396]

Karakas E, Truglio JJ, Croteau D, Rhau B, Wang L, Van Houten B, Kisker C. Structure of the C-terminal half of UvrC reveals an RNase H endonuclease domain with an Argonaute-like catalytic triad. EMBO J. 2007; 26:613–622. [PubMed: 17245438]

Lehmann AR. The xeroderma pigmentosum group D (XPD) gene: one gene, two functions, three diseases. Genes Dev. 2001; 15:15–23. [PubMed: 11156600]

Lloyd RS. Investigations of pyrimidine dimer glycosylases—a paradigm for DNA base excision repair enzymology. Mutat Res. 2005; 577:77–91. [PubMed: 15923014]

Machius M, Henry L, Palnitkar M, Deisenhofer J. Crystal structure of the DNA nucleotide excision repair enzyme UvrB from Thermus thermophilus. Proc Natl Acad Sci USA. 1999; 96:11717–11722. [PubMed: 10518516]

Malta E, Moolenaar GF, Goosen N. Dynamics of the UvrABC nucleotide excision repair proteins analyzed by fluorescence resonance energy transfer. Biochemistry. 2007; 46:9080–9088. [PubMed: 17630776]

Mazur SJ, Grossman L. Dimerization of Escherichia coli UvrA and its binding to undamaged and ultraviolet light damaged DNA. Biochemistry. 1991; 30:4432–4443. [PubMed: 1827034]

Nakagawa N, Sugahara M, Masui R, Kato R, Fukuyama K, Kuramitsu S. Crystal structure of Thermus thermophilus HB8 UvrB protein, a key enzyme of nucleotide excision repair. J Biochem. 1999; 126:986–990. [PubMed: 10578047]

Orren DK, Sancar A. The (A)BC excinuclease of Escherichia coli has only the UvrB and UvrC subunits in the incision complex. Proc Natl Acad Sci USA. 1989; 86:5237–5241. [PubMed: 2546148]

Orren DK, Sancar A. Formation and enzymatic properties of the UvrB.DNA complex. J Biol Chem. 1990; 265:15796–15803. [PubMed: 2168423]

Pakotiprapha D, Inuzuka Y, Bowman BR, Moolenaar GF, Goosen N, Jeruzalmi D, Verdine GL. Crystal structure of Bacillus stearothermophilus UvrA provides insight into ATP-modulated dimerization, UvrB interaction, and DNA binding. Mol Cell. 2008; 29:122–133. [PubMed: 18158267]

Pakotiprapha D, Liu Y, Verdine GL, Jeruzalmi D. A structural model for the damage-sensing complex in bacterial nucleotide excision repair. J Biol Chem. 2009; 284:12837–12844. [PubMed: 19287003]

Saffarian S, Collier IE, Marmer BL, Elson EL, Goldberg G. Interstitial collagenase is a Brownian ratchet driven by proteolysis of collagen. Science. 2004; 306:108–111. [PubMed: 15459390]

Sancar A. DNA excision repair. Annu Rev Biochem. 1996; 65:43–81. [PubMed: 8811174]

Sancar A, Rupp WD. A novel repair enzyme: UVRABC excision nuclease of Escherichia coli cuts a DNA strand on both sides of the damaged region. Cell. 1983; 33:249–260. [PubMed: 6380755]

Sancar A, Sancar GB. DNA repair enzymes. Annu Rev Biochem. 1988; 57:29–67. [PubMed: 3052275]

Schurr JM. The one-dimensional diffusion coefficient of proteins absorbed on DNA. Hydrodynamic considerations Biophys Chem. 1979; 9:413–414.

Skorvaga M, DellaVecchia MJ, Croteau DL, Theis K, Truglio JJ, Mandavilli BS, Kisker C, Van Houten B. Identification of residues within UvrB that are important for efficient DNA binding and damage processing. J Biol Chem. 2004; 279:51574–51580. [PubMed: 15456749]

Slutsky M, Mirny LA. Kinetics of protein-DNA interaction: facilitated target location in sequence-dependent potential. Biophys J. 2004; 87:4021–4035. [PubMed: 15465864]

Sohi M, Alexandrovich A, Moolenaar G, Visse R, Goosen N, Vernede X, Fontecilla-Camps JC, Champness J, Sanderson MR. Crystal structure of Escherichia coli UvrB C-terminal domain, and a model for UvrB-uvrC interaction. FEBS Lett. 2000; 465:161–164. [PubMed: 10631326]

Tafvizi A, Huang F, Leith JS, Fersht AR, Mirny LA, van Oijen AM. Tumor suppressor p53 slides on DNA with low friction and high stability. Biophys J. 2008; 95:L01–L03. [PubMed: 18424488]

Takayama K, Salazar EP, Broughton BC, Lehmann AR, Sarasin A, Thompson LH, Weber CA. Defects in the DNA repair and transcription gene ERCC2(XPD) in trichothiodystrophy. Am J Hum Genet. 1996; 58:263–270. [PubMed: 8571952]

Theis K, Chen PJ, Skorvaga M, Van Houten B, Kisker C. Crystal structure of UvrB, a DNA helicase adapted for nucleotide excision repair. EMBO J. 1999; 18:6899–6907. [PubMed: 10601012]

Truglio JJ, Rhau B, Croteau DL, Wang L, Skorvaga M, Karakas E, DellaVecchia MJ, Wang H, Van Houten B, Kisker C. Structural insights into the first incision reaction during nucleotide excision repair. EMBO J. 2005; 24:885–894. [PubMed: 15692561]

Truglio JJ, Croteau DL, Van Houten B, Kisker C. Prokaryotic nucleotide excision repair: the UvrABC system. Chem Rev. 2006a; 106:233–252. [PubMed: 16464004]

Truglio JJ, Karakas E, Rhau B, Wang H, DellaVecchia MJ, Van Houten B, Kisker C. Structural basis for DNA recognition and processing by UvrB. Nat Struct Mol Biol. 2006b; 13:360–364. [PubMed: 16532007]

Van Houten B, Croteau DL, DellaVecchia MJ, Wang H, Kisker C. ‘Close-fitting sleeves’: DNA damage recognition by the UvrABC nuclease system. Mutat Res. 2005; 577:92–117. [PubMed: 15927210]

Verhoeven EE, Wyman C, Moolenaar GF, Goosen N. The presence of two UvrB subunits in the UvrAB complex ensures damage detection in both DNA strands. EMBO J. 2002; 21:4196–4205. [PubMed: 12145219]

von Hippel PH, Berg OG. On the specificity of DNA-protein interactions. Proc Natl Acad Sci USA. 1986; 83:1608–1612. [PubMed: 3456604]

von Hippel PH, Berg OG. Facilitated target location in biological systems. J Biol Chem. 1989; 264:675–678. [PubMed: 2642903]

Wagner K, Moolenaar G, van Noort J, Goosen N. Single-molecule analysis reveals two separate DNA-binding domains in the Escherichia coli UvrA dimer. Nucleic Acids Res. 2009; 37:1962–1972. [PubMed: 19208636]

Wang H, DellaVecchia MJ, Skorvaga M, Croteau DL, Erie DA, Van Houten B. UvrB domain 4, an autoinhibitory gate for regulation of DNA binding and ATPase activity. J Biol Chem. 2006; 281:15227–15237. [PubMed: 16595666]

Wang H, Tessmer I, Croteau DL, Erie DA, Van Houten B. Functional characterization and atomic force microscopy of a DNA repair protein conjugated to a quantum dot. Nano Lett. 2008; 8:1631–1637. [PubMed: 18444686]

Waters TR, Eryilmaz J, Geddes S, Barrett TE. Damage detection by the UvrABC pathway: crystal structure of UvrB bound to fluorescein-adducted DNA. FEBS Lett. 2006; 580:6423–6427. [PubMed: 17097086]

Wolski SC, Kuper J, Hänzelmann P, Truglio JJ, Croteau DL, Van Houten B, Kisker C. Crystal structure of the FeS cluster-containing nucleotide excision repair helicase XPD. PLoS Biol. 2008; 6:e149. [PubMed: 18578568]

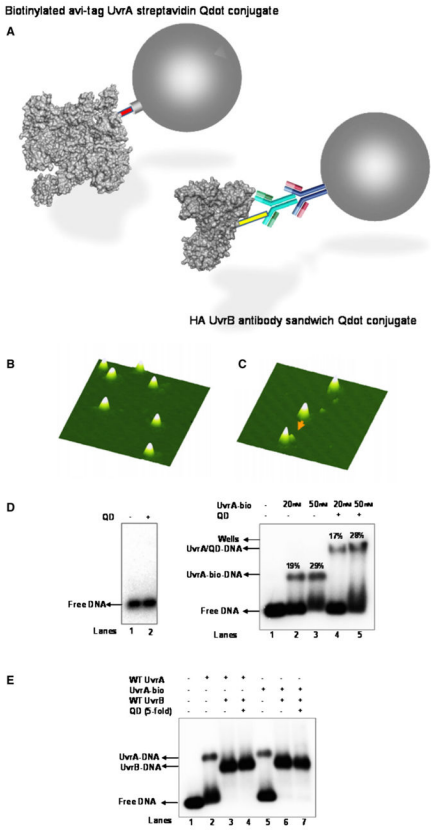

Figure 1. Qdot Labeling of UvrA and UvrB

(A) Attachment to UvrA was achieved through the biotinylation of UvrA using Avitag technology (see Supplemental Information) to which a streptavidin-coated Qdot was attached. For UvrB, we employed an antibody sandwich to distinguish the labeling strategies, thus permitting the inclusion of both labeled proteins in the same assay without crosstalk.

(B and C) AFM images of streptavidin-coated Qdots alone (B) and Qdots in the presence of UvrA-bio (C). Orange arrow points to a UvrA conjugated to a Qdot. The AFM image sizes are 400 × 400 nm at 15 nm height scale.

(D) Qdots do not bind to DNA (left). The addition of Qdots had no effect on the migration through an agarose gel of the target DNA. On the right, EMSA shows binding of UvrA and UvrA-Qdots to a fluorescein-containing DNA substrate where fluorescein serves as a lesion.

(E) EMSA showing that conjugation of UvrA to a Qdot does not affect its ability to load UvrB.

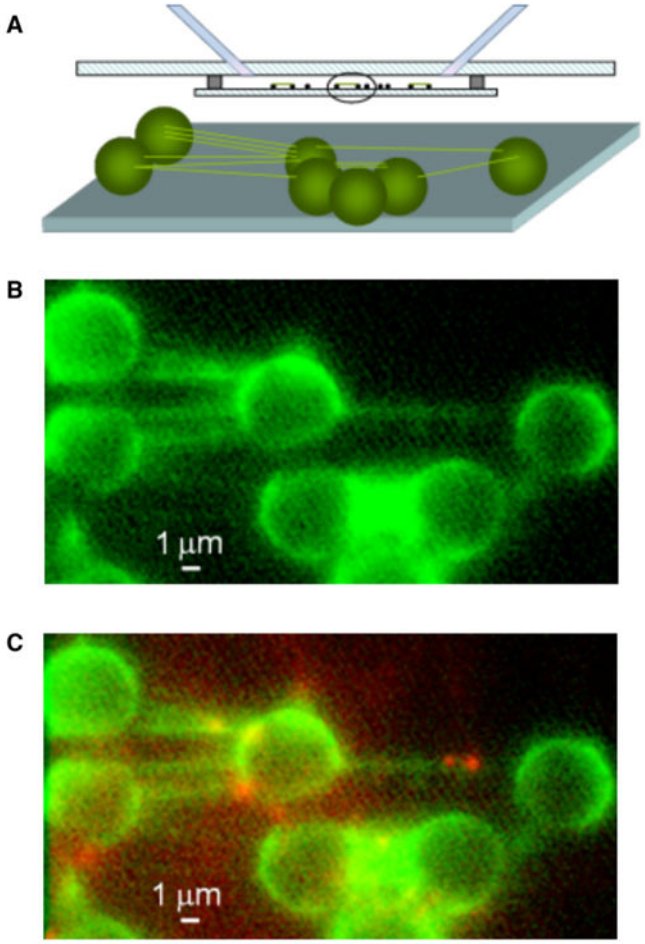

Figure 2. Experimental Layout of DNA Tightropes within a Flowcell

(A) A cross-section of the flowcell showing the placement of the inlet and outlet tubes into a standard microscope slide. A syringe pump attached to the tubes was used to withdraw solutions placed into an external reservoir; this permitted solution changes to be made rapidly and easily without disruption to flow. The tightropes were assembled in situ by the successive addition of the components required (see Experimental Procedures). Once assembled and washed, Qdot-labeled proteins could be introduced. During experiments, no flow was applied. In the lower panel, a 3D representation of a series of DNA tightropes is shown.

(B) Actual image of the surface (scale bar represents 1 μm) clearly showing the DNA tightropes labeled with YOYO-1 dye.

(C) Imaging UvrA bound to DNA. The same sample region from Figure 2B is shown after UvrA-$Qdot_{655}$ has been introduced to the flowcell. UvrA binding is clearly seen as red spots on the green DNA strands.

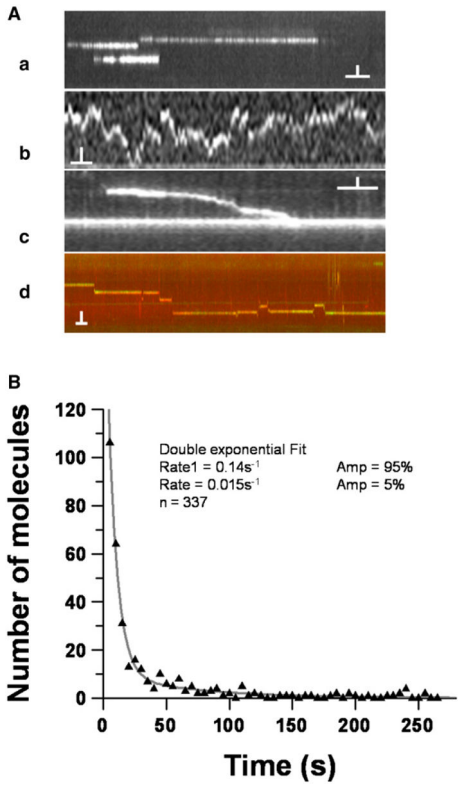

Figure 3. Analyzing the Binding of Uvr-Qdot Proteins to DNA Tightropes

(A) Kymographs of UvrAB complexes in motion. Four kymographs (a–d) are shown; these are unprocessed displacement versus time plots taken directly from the image files. Kymographs b–d originate from Movies S6–S8, respectively. Each vertical scale bar represents 1 μm (in subpanel d, 2 μm) and horizontal 5 s (in subpanel d, 10 s). Subpanel a shows a kymograph of a statically attached protein-Qdot to the DNA; the length of the "time streak" corresponds to the attached lifetime. Subpanel b shows unbiased free diffusion of the Uvr-Qdot protein complex corresponding to Movie S6. Subpanel c shows an example of Uvr-Qdot protein molecule with a directional bias to its diffusion (top trace), corresponding to Movie S7. Subpanel d shows an example of "paused motion," where molecules exhibit long pauses during their motion, corresponding to Movie S8. The total number of observations was 1221; 213 showed movement, and 1008 were static.

(B) The lifetime of UvrA binding to DNA. The lifetimes of 337 UvrA-Qdot molecules with characteristic horizontal time streaks across multiple experiments are plotted as a histogram and fitted to a double exponential, consistent with two Poisson processes. Given the very low amplitude of the second process (5%), we have ignored this in further analyses. The 95% amplitude signal indicates a detachment rate of 0.14 (± 0.01) s^{-1}. Therefore, on average, UvrA remains bound for ~7 s.

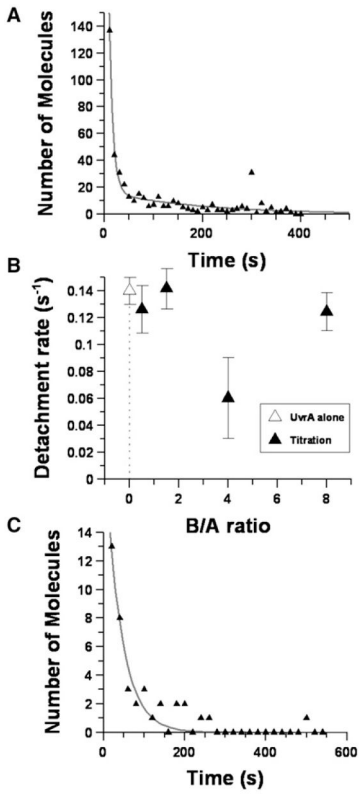

Figure 4. The Effects of UvrB on UvrA's Interaction with DNA

(A) Lifetime of UvrA-Qdot binding with UvrB present. The lifetimes of 449 molecules (with only UvrA labeled) across multiple experiments are plotted and fitted to a double exponential. As with UvrA alone, one process had a very low amplitude (<5%) and hence was ignored in further analyses. The larger amplitude signal indicates a detachment rate of 0.13 (± 0.02) s^{-1}. This difference is not sufficient to suggest an effect of UvrB binding on the attached lifetime of UvrA.

(B) Effect of different concentrations of UvrB on the detachment rate of UvrA. The analysis in (A) was performed across a range of UvrA/UvrB ratios, fixing the concentration of UvrA. Error bars are derived from exponential fits to lifetime histograms at the indicated UvrA/UvrB ratio.

(C) The attached lifetime of motile UvrAB complexes. UvrB was found to induce the motility of UvrA in the UvrAB complex (see main text). The lifetimes of complexes identified to be moving were plotted as a histogram and fit to a single exponential decay, yielding a detachment rate of 0.025 (± 0.003) s^{-1}, equivalent to an average lifetime of 40 s.

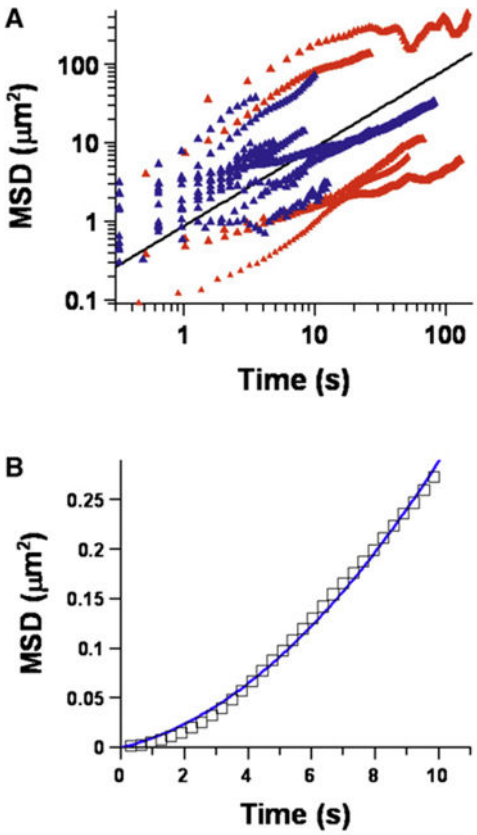

Figure 5. The Multiple Modes of UvrAB Complex Motion

(A) Mean squared displacement (MSD) plot of UvrAB complexes diffusing. The MSD was determined by calculating the squared distance moved during a prescribed time window. All data for that size window were averaged to produce a single point on the graph. The time window size was incrementally increased and the analysis reiterated to generate the time dependence of the mean displacement squared. The linear relationship is characteristic of unbiased diffusion. Data in blue represent each UvrA molecule (in the UvrAB complex) examined, and red represents the data originated from a dual-colored UvrAB complex. A log-log representation was used because the data were spread over orders of magnitude in time and displacement. A single origin-fixed linear regression gave a diffusion constant of 4.4 (± 0.2) × 10^{-4} $\mu m^2 s^{-1}$.

(B) Representative MSD plot for a molecule exhibiting directed motion. The mean squared displacement for a Qdot-labeled UvrAB complex with clear directed motion shows characteristic upward curvature when plotted with linear axes (in log-log space, a straight line with slope = 2 would be observed). These data were fit to a second order polynomial, the linear term revealed the unbiased diffusive component, and the quadratic term revealed the directed component. For this molecule, the values were 7.7 (± 0.7) × 0^{-3} $\mu m^2 s^{-1}$ and 2.1 (± 0.1) × 0^{-3} $\mu m s^{-1}$, respectively. The average diffusion for all of the data (n = 14) was 2.3 (± 1.2 SEM) × 0^{-3} $\mu m^2 s^{-1}$ and for the directed motion 1.3 (± 0.5 SEM) × 0^{-3} $\mu m s^{-1}$, equivalent to ~4 bps^{-1}.

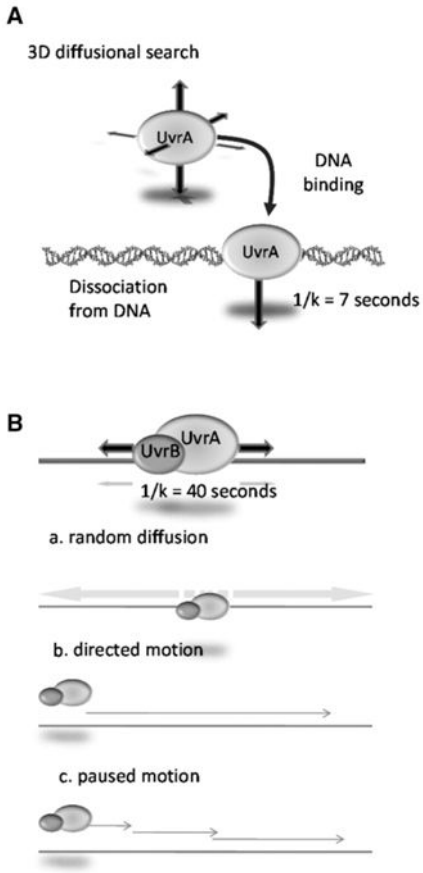

Figure 6. Summary of UvrA and UvrAB Motion

(A) UvrA (shown as a dimer) exhibits 3D searching with an average dwell time of 7 s on the DNA. UvrA can jump from one DNA molecule to another over long distances (~1 μm), but does not show any sliding.

(B) Of the UvrAB complexes on DNA, 17% showed movement. The movers had an average encounter time of 40 s and displayed three discrete types of motion: random diffusion, directed motion, and paused motion. Experiments presented here indicate that the UvrA dimer is capable of binding two independent UvrB molecules; however, the nature of the complex stoichiometry that underlies the different modes is unknown and currently under investigation. For an animated version of this figure, see Movie S10.

Table 1

Stoichiometry of UvrAB Complexes

			Number of Observations		
Proteins	**DNA**	**Qdot Label**	**Red**	**Green**	**Yellow**[b]
-	−	Alone[c]	3223	464	26 (2.7%)[d]
UvrB	−	UvrB	1738	404	74 (7.7%)[d,e,f]
UvrA + UvrB	−	UvrB	454	270	197 (21%)[e]
UvrA[a]	+	UvrA	115	67	127 (33%)
UvrA + UvrB	+	UvrB	56	37	38 (25%)[f]

The stoichiometry of UvrAB complexes was determined in the presence and absence of DNA. The latter was achieved by introducing a sample preincubated with excess $Qdot_{565}$ (green) and $Qdot_{655}$ (red) into a flowcell followed by immediate wash-through of buffer. This was performed to prevent surface saturation with Qdots and to ensure that the proteins bound to the surface reflected the population that was initially present when the sample was flowed in. Due to the large dilution upon introduction to the flow-chamber, the lack of a wash-though would provide a time-averaged view of the sample that would show a greater number of monomers. With DNA tightropes, this was not necessary, since the DNA was elevated from the surface, resulting in a lower background, and the dilutions were not excessive. The large excess of red over green Qdots was due to the experimental procedure where Qdots visible in the red channel were used as a cue to begin recordings. Given this large excess of red Qdots, we calculated an upper estimate of the percent yellow population in our controls by generating a total population from the number of green Qdots only, thus preventing our data being skewed by the greater number of red Qdots.

[a] Zero ATP.

[b] Percentage of yellow relative to the total Qdots capable of forming a complex (i.e., 2 × green + 2 × yellow) shown in parentheses.

[c] No Qdots bind to DNA in the absence of Uvr proteins.

[d] Significantly different (chi-square test: $p < 0.001$).

[e] Significantly different (chi-square test: $p < 0.001$).

[f] Significantly different (chi-square test: $p < 0.001$).